THE JOURNAL OF BIOLOGICAL CHEMISTRY VOL. 289, NO. 18, pp. 12264–12274, May 2, 2014

Structural Basis for Ovarian Tumor Domain-containing Protein 1 (OTU1) Binding to p97/Valosin-containing Protein (VCP)*

Received for publication, October 3, 2013, and in revised form, February 27, 2014 Published, JBC Papers in Press, March 7, 2014, DOI 10.1074/jbc.M113.523936

Su Jin Kim[‡§], Jinhong Cho[‡], Eun Joo Song[‡], Soo Jin Kim[¶], Ho Min Kim[¶], Kyung Eun Lee[‡], Se Won Suh[§1], and Eunice EunKyeong Kim[‡2]

From the [‡]Biomedical Research Institute, Korea Institute of Science and Technology, Seoul 136-791, Republic of Korea, [§]Department of Chemistry, College of Natural Sciences, Seoul National University, Seoul 151-747, Republic of Korea, and [¶]Graduate School of Medical Science and Engineering, Korea Advanced Institute of Science and Technology, 335 Gwahangno, Daejeon, 305-701, Republic of Korea

Background: Ovarian tumor domain-containing protein 1 (OTU1) acts as a deubiquitinating enzyme in the endoplasmic reticulum-associated degradation (ERAD) pathway by associating with valosin-containing protein (VCP).
Results: One OTU1 binds to a VCP hexamer with a K_D of 0.71 μM.
Conclusion: The ^{39}GYPP^{42} (S3/S4) loop of OTU1 is critical for interaction with VCP.
Significance: This is the first structural study of VCP and OTU1 complex.

Valosin-containing protein (VCP), also known as p97, is an AAA$^+$ ATPase that plays an essential role in a broad array of cellular processes including the endoplasmic reticulum-associated degradation (ERAD) pathway. Recently, ERAD-specific deubiquitinating enzymes have been reported to be physically associated with VCP, although the exact mechanism is not yet clear. Among these enzymes is ovarian tumor domain-containing protein 1 (OTU1). Here, we report the structural basis for interaction between VCP and OTU1. The crystal structure of the ubiquitin regulatory X-like (UBXL) domain of OTU1 ($UBXL_{OTU1}$) complexed to the N-terminal domain of VCP (N_{VCP}) at 1.8-Å resolution reveals that $UBXL_{OTU1}$ adopts a ubiquitin-like fold and binds at the interface of two subdomains of N_{VCP} using the ^{39}GYPP^{42} loop of $UBXL_{OTU1}$ with the two prolines in *cis*- and *trans*-configurations, respectively. A mutagenesis study shows that this loop is not only critical for the interaction with VCP but also for its role in the ERAD pathway. Negative staining EM shows that one molecule of OTU1 binds to one VCP hexamer, and isothermal titration calorimetry suggests that the two proteins bind with a K_D of 0.71 μM. Analytical size exclusion chromatography and isothermal titration calorimetry demonstrates that OTU1 can bind VCP in both the presence and absence of a heterodimer formed by ubiquitin fusion degradation protein 1 and nuclear localization protein 4.

Protein degradation is required for the elimination of faulty or unnecessary proteins as the accumulation or deposition of these proteins leads to various human diseases such as diabetes, inflammation, and neurodegenerative disorders (1). The endoplasmic reticulum-associated degradation (ERAD)[3] pathway in particular serves to maintain endoplasmic reticulum homeostasis in the lumen or the membrane of the endoplasmic reticulum and belongs to the ubiquitin-proteasome pathway requiring two catalyzing processes, ubiquitination and deubiquitination (2). This pathway comprises three stages: the recognition of aberrant proteins, the retrotranslocation of the ubiquitin-modified substrates from the endoplasmic reticulum to the cytosol, and the degradation by the proteasome (3).

One of the many players in the ERAD pathway, valosin-containing protein (VCP; also known as p97 in mammals and CDC48 in yeast) is an abundant, highly conserved, and essential AAA$^+$ ATPase. VCP governs critical steps such as retrotranslocation and transportation of substrates to the proteasome (4), and it recognizes its substrates mostly in the presence of the ubiquitin-fusion degradation protein 1 (UFD1)/nuclear localization protein 4 (NPL4) heterodimer (5). It comprises an N-terminal domain, two ATPase domains (D1 and D2), and a C-terminal tail. It forms a homohexameric ring structure with D1 and D2 stacked in a head to tail manner, and the N-terminal domains are enclosed by the D1 ring (7). In addition to the ERAD pathway, VCP is associated with a large number of independent cellular processes including transcription activation, mitosis, apoptosis, DNA repair, autophagy, endosomal sorting, and protein degradation at the outer mitochondrial membrane (see Refs. 8 and 9 and references therein). These functions are

* This work was supported by Global Research Laboratory Program Grant 2013056409 of the Ministry of Science, Information and Communication Technology and Future Planning of Korea and an institutional grant from the Korea Institute of Science and Technology.

The atomic coordinates and structure factors (codes 4KDI and 4KDL) have been deposited in the Protein Data Bank (http://wwpdb.org/).

[1] To whom correspondence may be addressed. Tel.: 82-2-880-6653; Fax: 82-2-958-6813; E-mail: sewonsuh@snu.ac.kr.

[2] To whom correspondence may be addressed. Tel.: 82-2-880-6601; Fax: 82-2-958-5909; E-mail: eunice@kist.re.kr.

[3] The abbreviations used are: ERAD, endoplasmic reticulum-associated degradation; OTU, *ovarian tumor;* OTU1, ovarian tumor domain-containing protein 1; VCP, valosin-containing protein; ITC, isothermal titration calorimetry; UFD1, ubiquitin fusion degradation protein 1; NPL4, nuclear localization protein 4; UBX, ubiquitin regulatory X; UBXL, ubiquitin regulatory X-like; RPN-I, ribophorin I; Ni-NTA, nickel-nitrilotriacetic acid; FAF1, Fas-associated factor 1; UBD, ubiquitin D domain; r.m.s.d., root mean square deviation; K_D, binding affinity; VCIP135, VCP complex-interacting protein of 135 kDa.

dependent on a multitude of regulatory binding partners of VCP that interact with the N-terminal domain and/or the C-terminal tail of VCP; these binding partners can be classified as either substrate-recruiting or substrate-processing proteins (10). Defects in VCP or its binding partners have been linked to several diseases (8, 9).

Recently, a number of ERAD-specific deubiquitinating enzymes have been reported to be physically associated with VCP (11, 12). Among these enzymes is ovarian tumor domain-containing protein 1 (OTU1). OTU1 is known as a deubiquitinating enzyme as well as a substrate-processing factor of VCP that is required for the retrotranslocation of the ERAD pathway (13). It also plays a role in controlling ubiquitinated or unubiquitinated substrates in the ERAD pathway (14). However, the exact mechanisms are not yet well understood. It harbors three domains: an N-terminal ubiquitin regulatory X-like (UBXL) domain, an OTU domain, and a C-terminal zinc finger domain of unknown function. It binds to the N-terminal domain of VCP (N_{VCP}) through the UBXL domain and removes ubiquitin chains using the OTU domain (15). In particular, the UBXL domain of OTU1 ($UBXL_{OTU1}$) consists of about 80 residues similar to the ubiquitin regulatory X (UBX) domain, which is one of the best characterized adaptor domains of VCP. UBX interacts with N_{VCP} via a conserved arginine from strand β1 and the three residues (Phe-Pro-Arg) in a four-residue-long loop formed between strands β3 and β4 often referred to as the S3/S4 loop (16, 17). These residues, "R . . . FPR," form the signature motif of UBX. However, UBXL has low sequence identity of less than 15% to UBX and furthermore lacks the signature motif of UBX. So far, the structure of the OTU domain from yeast complexed with ubiquitin has been produced (18), and recently it has been demonstrated that YOD1, the mammalian homolog of OTU1, has high specificity for Lys^{11}-linked ubiquitin chains in a report that shows the complex structure of YOD1 with Lys^{11}-linked diubiquitin (19). To understand how OTU1 interacts with VCP on a molecular level and to gain insight into how this interaction regulates the ERAD pathway, we carried out a structural study on N_{VCP} complexed with $UBXL_{OTU1}$ and performed negative staining electron microscopy (EM) and biochemical studies of the full-length proteins.

EXPERIMENTAL PROCEDURES

Cloning, Mutagenesis, and Protein Preparation—All human VCP and yeast OTU1 proteins were cloned into the expression vector pET28a (Novagen) that appends an N-terminal histidine tag and thrombin site to the target protein under T7 promoter control. Substitution of Gly-Tyr-Pro-Pro to Thr-Phe-Pro-Arg at positions 39–42 of the full-length OTU1 (residues 1–301) was introduced by a PCR method in clone OTU1 ^{39}TFPR^{42}. For expression in mammalian cells, the constructs encoding pCS2-HA-OTU1 WT and pCS2-HA-OTU1 ^{39}TFPR^{42} were prepared. A ribophorin I mutant (RPN-I^{N299T}) with the asparagine at position 299 replaced by threonine was cloned into the pEGFP-C1 vector (Clontech). For analytical size exclusion chromatography, the full-length UFD1 (residues 1–307) and NPL4 (residues 1–608) were cloned into the pET28a and pET22b vectors (Novagen), respectively, which are named pET28a-UFD1 and pET22b-NPL4. The glutathione *S*-transferase (GST) protein was fused to the N terminus of the full-length OTU1, and pGST-OTU1 was derived from pGEX-4T-1 (GE Healthcare). All proteins were expressed in *Escherichia coli* Rosetta (DE3). Cells were grown in LB medium at 37 °C, and protein expression was induced by 0.5 mM isopropyl β-D-1-thiogalactopyranoside at 18 °C overnight. Harvested cells were lysed in buffer A (20 mM Tris hydrochloride, pH 8.0, 100 mM sodium chloride, 0.5 mM tris(2-carboxyethyl)phosphine with 1 mM PMSF) and purified using nickel-nitrilotriacetic acid (Ni-NTA) affinity chromatography (GE Healthcare). Afterward, the histidine tag was proteolytically cleaved by addition of thrombin (Enzyme Research Laboratories), and protein was further purified using size exclusion chromatography on a HiLoad Superdex 75 or 200 26/60 column (GE Healthcare) in buffer A or buffer B (20 mM HEPES, pH 7.5, 150 mM sodium chloride). 2 mM ATP and 5 mM magnesium chloride were added to the full-length VCP (residues 1–806). A UFD1/NPL4 heterodimeric complex was formed by mixing pET28a-UFD1 and pET22b-NPL4. For the formation of complexes using the full-length proteins, VCP and either OTU1 (VCP/OTU1) or UFD1/NPL4 (VCP·UFD1/NPL4) were incubated at a molar ratio of 1:3 for 1 h at 4 °C, and then VCP/OTU1 and VCP·UFD1/NPL4 complexes were analyzed by size exclusion chromatography.

Limited Proteolysis of the Complex of N_{VCP} and $UBXL_{OTU1}$—Purified complexes of N_{VCP} and $UBXL_{OTU1}$ were digested with chymotrypsin and trypsin (Sigma) at a protein-to-protease ratio of 1,000:1 in buffer A for 15 and 5 min, respectively, at 37 °C. The reactions were stopped by addition of 0.1 mM PMSF. Reaction products were resolved by 15% SDS-PAGE and visualized by subsequent Coomassie Brilliant Blue staining. The proteins were used at a concentration of 20 mg/ml for crystallization.

Crystallization of the VCP and OTU1 Complex—Crystals of crystal form I were obtained from a reservoir solution containing 14% PEG 4000, 100 mM sodium acetate, pH 5.0, and those of crystal form II were obtained from 20% PEG 2000, 10% tacsimate, pH 5.0 using the hanging drop vapor diffusion method by mixing with an equal volume of the protein solution. Crystals in a soaking solution containing 25% ethylene glycol as a cryoprotectant were flash cooled in liquid nitrogen.

Data Collection and Structure Determination—Diffraction data of the two crystal forms were collected at 100 K on beamline 5C of Pohang Light Source, Republic of Korea. The data were processed and scaled using the program suite HKL2000 (20). Crystal form I in the asymmetric unit was located by molecular replacement using the program Phaser (21) with the free VCP structure (Ref. 22; Protein Data Bank code 1E32) as a search model. The structure of crystal form II was subsequently determined using the refined structure of crystal form I as an input model. Iterative model building was performed by manually fitting into the unoccupied densities with Coot (23), and refinement was carried out by CNS (24), PHENIX (25), and REFMAC5 (26). Water molecules were added with Coot, and structures of the two crystal forms were validated using PROCHECK (27). Coordinates of the crystal structures have been deposited in the Protein Data Bank under codes 4KDI and 4KDL. All figures were generated with PyMOL (28). The data

collection and processing statistics for the two structures are summarized in Table 1.

Chemical Cross-linking—VCP·UFD1/NPL4 complex was purified and concentrated to 0.05 mg/ml in buffer B. To improve its stability, the complex was chemically cross-linked with a final concentration of 0.1% EM grade glutaraldehyde (Sigma) for 10 min at 25 °C. The reaction was stopped by adding Tris, pH 8.0 to a final concentration of 25 mM.

Isothermal Titration Calorimetry (ITC) Measurements—ITC experiments were performed on an iTC200 calorimeter (GE Healthcare) at 25 °C. For the interaction between the full-length VCP and OTU1, OTU1 wild type (WT) or the mutant (^{39}TFPR^{42}) was placed in the syringe at 300 or 500 μM, respectively, and injected into the sample cell containing the full-length VCP at a concentration of 13 μM. The concentration of VCP/OTU1 and VCP·UFD1/NPL4 complexes was 0.01 μM in the sample cell, and UFD1/NPL4 and OTU1 were titrated to a concentration of 20 μM. Buffer B always matched between the syringe and the sample cell. The data were analyzed with the software Origin 7.0 using a one-site model.

In Vitro Assays of Substrate Degradation—HEK293T cells were seeded onto 12-well poly-L-lysine-coated plates at a density of 2.5×10^5 cells/well, and then transfection with expression plasmids was performed for 2 days using Effectene reagent (Qiagen). The total amount of DNA used in each well for transfection was 600 ng. Cells were treated with 10 μM MG132 for 2 h to prevent protein degradation and washed twice with complete medium. After addition of cycloheximide at a final concentration of 100 μg/ml, cells were harvested with cold Dulbecco's phosphate-buffered saline (PBS) and lysed, and cell extracts were analyzed by Western blotting with antibodies against pCS2-HA, pCS2-HA-OTU1 WT, pCS2-HA-OTU1 ^{39}TFPR^{42}, and pEGFP-C1-RPN-I^{N299T}.

Ni-NTA Nanogold Labeling of VCP and OTU1 Complex—The complex was prepared by co-purifying the full-length untagged VCP and OTU1 tagged with a hexahistidine tag at the C terminus. Freshly purified protein complex and 5-nm-diameter Ni-NTA Nanogold (Nanoprobes Inc.) were incubated together at a molar ratio of 1:10 for 10 min at 4 °C. The mixture was purified with a further chromatographic step using a Superdex 200 10/300 GL column (GE Healthcare) in buffer A. Excess Ni-NTA Nanogold was removed by centrifugation at $3,000 \times g$ for 15 min using a 10-kDa-cutoff filter (Sartorius).

EM—The complex of the full-length VCP and OTU1 (VCP/OTU1) labeled with gold was diluted to 20 μg/ml in buffer A. The samples were loaded onto a glow-discharged copper grid coated with a carbon film and stained with 2% uranyl acetate solution. Images were recorded on the film using a Tecnai F20 microscope operated at 200 kV equipped with a $2,048 \times 2,048$-pixel Gatan charge-coupled device camera. The gold-labeled proteins were selected from individual digital micrographs using a semiautomatic selection procedure, and the stoichiometry of OTU1 incorporation into VCP was determined by counting the number of gold particles. For unlabeled VCP/OTU1 complex, VCP/OTU1 complex was formed by incubating purified VCP with a 10-fold molar excess of OTU1 for 15 min at 4 °C. The complex was then further purified using size exclusion chromatography (GE Healthcare) in buffer containing 20 mM Tris hydrochloride, pH 8.0, 200 mM sodium chloride. 3 μl of VCP/OTU1 complex fraction at 0.1 μM was applied to a glow-discharged carbon-coated copper grid, and negatively stained with 2% methylamine vanadate, pH 8.0 (Nanoprobes Inc.). The specimen was examined under a Tecnai T120 microscope at 120 kV using a nominal magnification of 67,000× (1.64 Å/pixel; FEI Eindhoven, The Netherlands). Images were recorded with an FEI Eagle $4,000 \times 4,000$-pixel charge-coupled device camera using a defocus of 1.2 μm and an electron dose of about 30 e^-/A^2.

EM Image Processing—Because VCP has a preferred orientation on the EM grid, we could only obtain the hexagonal view of VCP or VCP/OTU1 complex. Hexagonal particles were automatically selected with EMAN2 boxer, and bad particles were manually excluded (29). A total of 2,839 particles were selected from 50 micrographs. Subsequent processing was performed using IMAGIC (30). To separate VCP/OTU1 complex from the heterogeneous data set containing either VCP or VCP/OTU1 complex, we executed comparative projection matching with two reference sets. One reference set was the forward projection of the crystal structure of VCP hexamer (Ref. 31; Protein Data Bank code 1R7R), and the other reference set was the forward projection of the model structure of VCP hexamer with one OTU1 molecule (Protein Data Bank codes 4KDI and 4KDL in the present work and 1R7R). These two separate data sets were respectively subjected to 10 rounds of reference-free alignment and multivariate statistical analysis followed by multivariate statistical analysis classification and averaging.

Analytical Size Exclusion Chromatography—pET28a-VCP, pGST-OTU1, pET28a-UFD1, and pET22b-NPL4 were expressed and purified separately. Analytical size exclusion chromatography was carried out at 4 °C on a Superdex 200 10/300 GL column (GE Healthcare) in buffer A at a flow rate of 0.5 ml/min. Elution fractions were analyzed for complexes by SDS-PAGE and Coomassie Brilliant Blue staining.

RESULTS AND DISCUSSION

Overall Structure of N_{VCP} and $UBXL_{OTU1}$ Complex—To obtain atomic details on the interaction between VCP and OTU1, a number of complexes of VCP and OTU1 using various fragments containing the full -length were subjected to crystallization trials (see Fig. 1*A*). However, only the complex of N_{VCP} and $UBXL_{OTU1}$ yielded diffraction quality crystals in two conditions: one with residues 21–196 and the other with residues 1–187 of N_{VCP}, referred to hereafter as crystal form I and crystal form II, respectively. Both crystal forms I and II crystallized in space group $P2_12_12_1$ but with $Z = 1$ and $Z = 2$, respectively, and were refined at 1.81- and 1.86-Å resolution, respectively. First, the molecular replacement method using various structures such as UBX of Fas-associated factor 1 (FAF1) (Protein Data Bank code 3QX1; denoted as UBX_{FAF1} hereafter) and the NMR structure of $UBXL_{OTU1}$ (Protein Data Bank code 2KZR) failed to give a solution. However, repeating the search using uncomplexed N_{VCP} (residues 21–187) (Ref. 22; Protein Data Bank code 1E32) as a search model gave a solution, and the subsequent $F_o - F_c$ difference electron density map revealed unambiguous density for bound OTU1. The structure of crystal form II was determined by the molecular replacement method using

the structure of crystal form I. Residues that were not visible in the electron density map were left out in the final model; they include residues 1–20 of N_{VCP} in all three molecules, 121–128 of N_{VCP} in one molecule from crystal form II, 48–52 of $UBXL_{OTU1}$ in crystal form I, and 49–55 in one molecule of $UBXL_{OTU1}$ from crystal form II. The statistics on data collection and the refinements are given in Table 1.

The overall structure of the N_{VCP} and $UBXL_{OTU1}$ complex is shown in Fig. 1*B*. As seen in the figure, N_{VCP} is composed of two subdomains (N1 and N2) connected by a seven-residue-long linker, and $UBXL_{OTU1}$ binds at the interface between the N1 and N2 domains of VCP. The N1 domain (residues 23–104) consists of a double-Ψ β-barrel, and the N2 domain (residues 112–196) consists of a six-stranded β-clam with two helices on

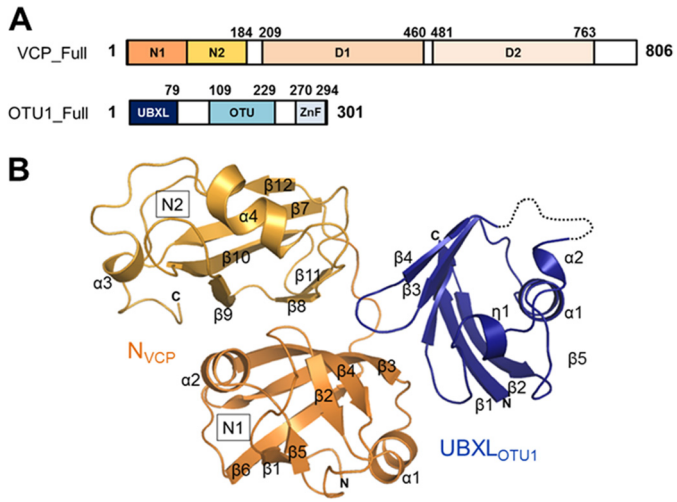

FIGURE 1. **Crystal structure of the N_{VCP} and $UBXL_{OTU1}$ complex.** *A*, schematic representation of domain structures of VCP and OTU1. *B*, ribbon presentation of $UBXL_{OTU1}$ in complex with N_{VCP} shown in *blue* and *orange*, respectively. Secondary structure elements are labeled: α for α-helix, β for β-strand, and η for 3_{10}-helix. Disordered regions are indicated by *dotted lines*. *ZnF*, zinc finger.

the two ends as described earlier (7). The structure of $UBXL_{OTU1}$ (residues 1–73) reveals a β-grasp fold with a β-β-α-β-β-α-α-β secondary structural organization that resembles ubiquitin and ubiquitin-like proteins as well as UBX and the ubiquitin D domain (UBD) (18, 32). However, it differs significantly, especially in the conformation of the loops and the electrostatic surface, and these differences will be discussed later.

The three crystallographically independent molecules, one from crystal form I and two from crystal form II, are almost identical. When the molecule of crystal form I is taken as a reference, the two molecules in crystal form II show root mean square deviation (r.m.s.d.) values of 0.63 and 0.64 Å for N_{VCP} and 0.45 and 0.50 Å for $UBXL_{OTU1}$. When compared with N_{VCP} used in the search model, the r.m.s.d. varies from 0.49 to 0.54 Å, suggesting that there are no structural changes upon binding of $UBXL_{OTU1}$. In the case of N_{VCP}, residues 33–34, 119–129, 155–159, and 182–187 show r.m.s.d. values greater than 3 Å, but they are typically located on the surface away from the binding interface with $UBXL_{OTU1}$. These high r.m.s.d. values are due to differences in the crystal packing environment or flexibility of the molecule (data not shown). Residues 46–56 are ordered in only one of the three $UBXL_{OTU1}$ molecules because there is a neighboring molecule stabilizing the structure by forming hydrogen bonds (data not shown). Conversely, the superposition of $UBXL_{OTU1}$ with the earlier reported NMR structure (Protein Data Bank code 2KZR) gives an r.m.s.d. of 2.18 Å for 73 Cα atoms; this might be the reason for the failure to obtain a solution using the structure as a search model.

Comparison of $UBXL_{OTU1}$ with UBX/UBD—A DALI search using $UBXL_{OTU1}$ as a search model gave UBX_{FAF1} (Protein Data Bank code 3QX1) as the closest match with a *Z*-score of 8.8, r.m.s.d. of 1.9 Å (68 Cα atoms), and sequence identity of 13%. FAF1 is a ubiquitin receptor containing multiple ubiquitin-related domains that is involved in various physiological functions such as apoptosis and NF-κB signaling. The second

TABLE 1
Data collection and refinement statistics
Values in parentheses are for the highest resolution shell.

	Crystal form I	Crystal form II
Data sets		
Beam line	PAL 5C (SB II)	PAL 5C (SB II)
X-ray wavelength (Å)	0.97951	0.97951
Resolution range (Å)	50.00–1.81 (1.87–1.81)	50.00–1.86 (1.93–1.86)
Space group	$P2_12_12_1$	$P2_12_12_1$
Unit cell parameters (Å; °)	$a = 43.604$, $b = 60.803$, $c = 111.915$; $\alpha = 90.000$, $\beta = 90.000$, $\gamma = 90.000$	$a = 42.819$, $b = 88.609$, $c = 143.535$; $\alpha = 90.000$, $\beta = 90.000$, $\gamma = 90.000$
Z	1	2
Total/unique reflections (*N*)	684,606/27,896	1,413,706/46,883
Completeness (%)	99.3 (99.6)	96.5 (88.9)
Mean I/σ (%)	23.8 (8.9)	25.0 (2.6)
R_{merge} [a] (%)	9.1 (25.2)	8.9 (38.5)
Refinement statistics		
No. of atoms	2,206	3,872
No. of water molecules	272	198
Resolution range (Å)	33.78–1.81	42.34–1.86
R/R_{free} [b] (%)	18.24/21.34	21.37/25.68
r.m.s.d. bond length (Å)/angle (°)	0.026/2.145	0.023/1.926
Average *B*-factor (Å^2)	18.98	30.61
Ramachandran plot		
Favored region (%)	98.7	96.7
Allowed region (%)	1.3	3.3
Disallowed region (%)	0	0

[a] $R_{merge} = \Sigma_h\Sigma_i|I(h,i)|I(h)|/\Sigma_h\Sigma_i I(h,i)$ where $I(h,i)$ is the intensity of the *i*th measurement of reflection *h* and $I(h)$ is the mean value of $I(h,i)$ for all *i* measurements.
[b] R_{free} was calculated from the randomly selected 10% set of reflections not included in the calculation of the *R* value.

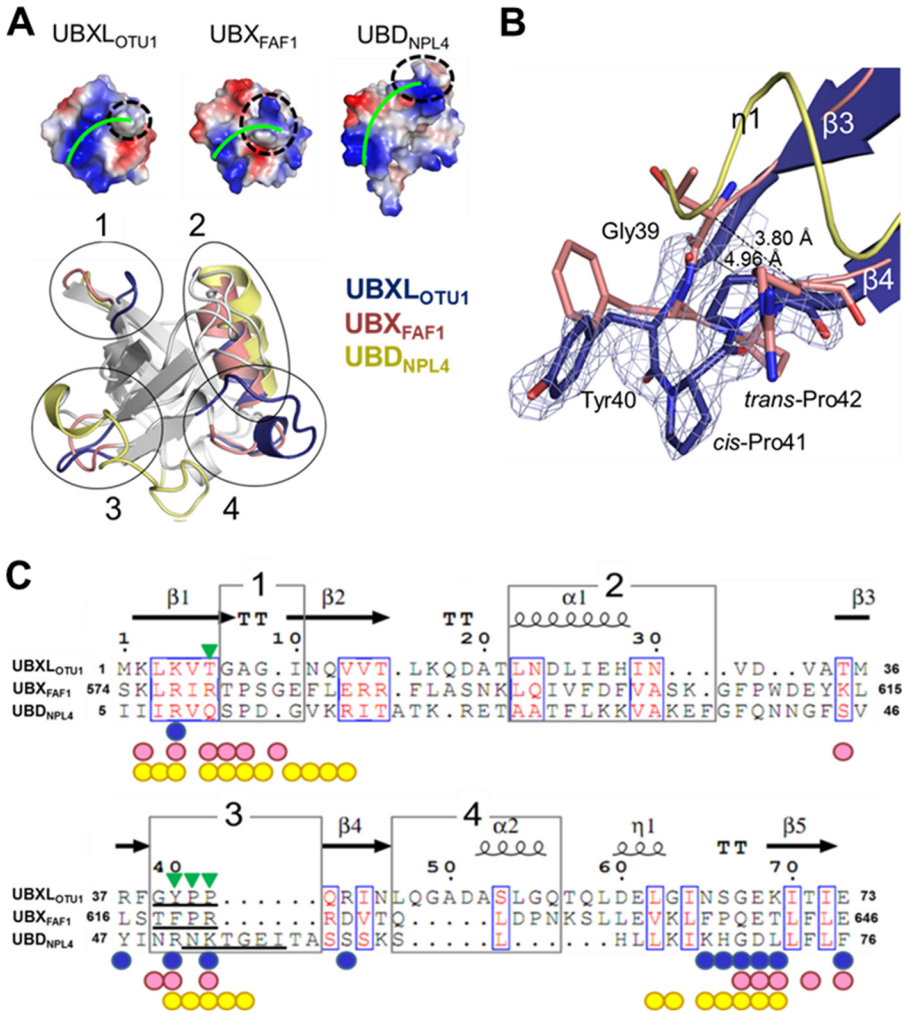

FIGURE 2. **Comparison of UBXL$_{OTU1}$ with UBX$_{FAF1}$ and UBD$_{NPL4}$.** *A*, the surface showing electrostatic charges of UBXL$_{OTU1}$, UBX$_{FAF1}$, and UBD$_{NPL4}$ with *red* representing negatively charged surface and *blue* representing positively charged surface (*top*). Superposition of the three structures is also shown (*bottom*). The S3/S4 loop of UBXL$_{OTU1}$ and UBX$_{FAF1}$ and 3_{10}-helix of UBD$_{NPL4}$ are *circled*, and the binding region for N$_{VCP}$ is marked by a *green line*. Four regions (*1–4*) with significant differences are indicated by *circles*. *B*, the electron density map ($2F_o - F_c$) of crystal form I is shown at the 1.5σ level. *C*, structure-based sequence alignment of UBXL$_{OTU1}$, UBX$_{FAF1}$, and UBD$_{NPL4}$ with the secondary structural elements of UBXL$_{OTU1}$ shown *above* the sequence, and α, β, η, and TT denote α-helix, β-strand, 3_{10}-helix, and β-turn, respectively. Well conserved residues are *boxed*, and the predominant residues shown in *red*. Residues of the signature motif of UBX are marked by *green inverted triangles*. The four regions in *A* are highlighted by *boxes*. Residues involved in N$_{VCP}$ binding are indicated by a *colored circle below* the sequence. The color code is the same as in *A*. The alignment was generated by STRAP (6) and ESPript (49).

best match was ubiquitin (Ref. 33; Protein Data Bank code 1YIW) with a *Z*-score of 8.2, r.m.s.d. of 2.2 Å (63 Cα atoms), and sequence identity of 12%. Other ubiquitin-like proteins such as NEDD8 (Protein Data Bank code 3GZN), SUMO-1 (Protein Data Bank code 1A5R), SMT3 (Protein Data Bank code 3V62), and FUB1 (Protein Data Bank code 2L7R) showed *Z*-scores slightly less than 8, and they all had similar sequence identities as well. UBD of NPL4-like protein (Protein Data Bank code 1WF9) showed a *Z*-score of around 5. Although the function of NPL4-like protein is not yet clear, UBD of NPL4 (Ref. 34; Protein Data Bank code 2PJH; UBD$_{NPL4}$) has been reported to assist VCP along with UFD1 in the ERAD pathway (5). Thus, it is included in the following comparison instead.

Fig. 2 shows a comparison of UBXL$_{OTU1}$ with UBX$_{FAF1}$ (Ref. 35; Protein Data Bank code 3QQ8) and UBD$_{NPL4}$ along with the structure-based sequence alignment using the alignment program STRAP (6). The r.m.s.d. obtained in the superposition of UBXL$_{OTU1}$ and UBX$_{FAF1}$ (UBD$_{NPL4}$) is 2.21 Å (3.97 Å) for 73 Cα atoms. Although these proteins, namely UBXL$_{OTU1}$, UBX$_{FAF1}$, and UBD$_{NPL4}$, share structural homology at the Cα level, the electrostatic surfaces are quite different (Fig. 2*A*). The electrostatic surface of UBXL$_{OTU1}$ is particularly distinct: one side shows a positively charged patch, whereas the opposite side shows a broad negatively charged patch. The positively charged patch is formed by Lys^{2}, Lys^{4}, Arg^{37}, Arg^{44}, and Lys^{69} from the various strands of the β-sheet, whereas the negatively charged patch is formed by residues such as Asp^{24}, Glu^{27}, Asp^{60}, and Glu^{61} from α1 and η1 of UBXL$_{OTU1}$ (data not shown).

Despite the fact that the overall structures are similar, a detailed comparison reveals differences in four particular regions, and these are highlighted in Fig. 2, *A* and *C*. The four regions are well defined in the electron density maps and are almost the same in all three structures of crystal forms I and II. First, the β1-β2 loop, highlighted the region 1 of Fig. 2*A*, is tilted more toward the body of the molecule by about 20° in UBXL$_{OTU1}$. Second, the α1 helix of UBXL$_{OTU1}$ is shorter than

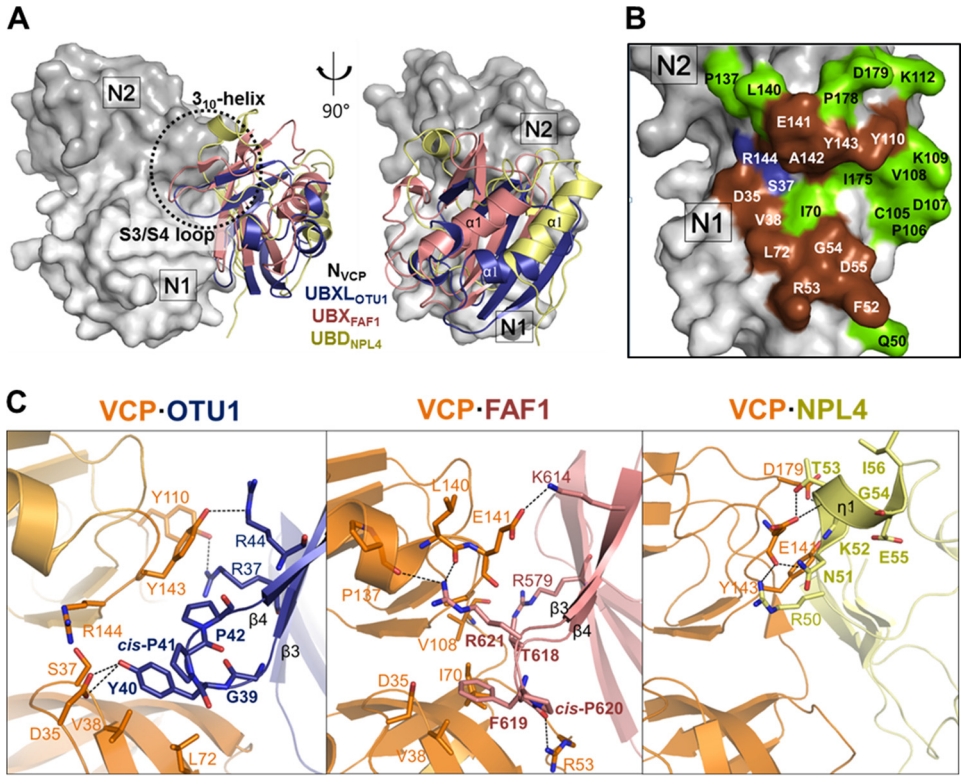

FIGURE 3. **Analysis of interaction between N_{VCP} and binding partners.** *A*, superposition of the complex structures of VCP·OTU1 (crystal form I in this study), VCP·FAF1 (Ref. 35; Protein Data Bank code 3QQ8), and VCP·NPL4 (Ref. 34; Protein Data Bank code 2PJH) shown in *blue*, *pink*, and *yellow*, respectively. Only N_{VCP} was used for superposition. N_{VCP} is shown in surface representation, whereas binding partners are shown in ribbon representation. *B*, binding surface of N_{VCP}. The region that all three binding partners bind is colored in *brown*, whereas the region unique to $UBXL_{OTU1}$ binding is shown in *blue*, and the region that is irrelevant to $UBXL_{OTU1}$ binding but important in UBX_{FAF1} and UBD_{NPL4} is shown in *green*. *C*, details of the interaction between N_{VCP} and binding partners. The interactions formed around the S3/S4 loop region (in *boldface*) of binding partners are shown with the key residues in stick presentation. Hydrogen bonds are indicated by *dashed lines*.

that of UBX_{FAF1} and UBD_{NPL4} by nearly one turn. This is due to deletion of four residues in $UBXL_{OTU1}$. In addition, $UBXL_{OTU1}$ has an additional α-helix formed by residues 53–56 with an insertion of five residues after β4 (region 4), and this region extends outward from the body of the molecule. In fact, it is about 11 Å away from the corresponding loop position of UBX_{FAF1}.

The most intriguing difference is the β3-β4 loop conformation of $UBXL_{OTU1}$ (region 3 in Fig. 2*A*). This loop corresponds to the S3/S4 loop, which is part of the signature motif of UBX. This loop is composed of Gly^{39}-Tyr^{40}-Pro^{41}-Pro^{42}, and all the residues are well defined in the electron density map as shown in Fig. 2*B*. The two prolines in this loop are found in the *cis*- and *trans*-configurations, respectively. The loop has a type VIb β-turn and is stabilized by intramolecular hydrogen bonds formed between Phe^{38} and Gln^{43} (N–O, 3.07 Å; O–N, 2.83 Å) as well as π-π stacking interactions between proline and the preceding tyrosine. This is quite similar to that of UBX_{FAF1}; *i.e.* the corresponding Thr-Phe-Pro-Arg forms a VIb β-turn, and the proline adopts a *cis*-configuration. However, the proline of UBX_{FAF1} does not form similar π-π stacking interactions with the preceding phenylalanine, and the distances between the first and the fourth Cα atoms in the loop are 4.96 and 3.80 Å in $UBXL_{OTU1}$ and UBX_{FAF1}, respectively, resulting in different conformations (Fig. 2*B*). This may be due to the additional proline in $UBXL_{OTU1}$. Conversely, the proline in the S3/S4 loop of UBX_{p47} was reported to be in *trans*-configuration (36). The corresponding region in UBD_{NPL4} is longer by six residues and forms a 3_{10}-helix instead of the loop as shown in Fig. 2*B*. Taken together, the structure of $UBXL_{OTU1}$ exhibits distinctive features from UBX_{FAF1} or UBD_{NPL4}, and these regions, especially regions 1 and 3, appear to serve as a platform for different interactions.

Comparison of Interaction between N_{VCP} and $UBXL_{OTU1}$/UBX_{FAF1}/UBD_{NPL4}—To understand how $UBXL_{OTU1}$ differs from UBX_{FAF1} and UBD_{NPL4} in N_{VCP} binding, the complex structure of N_{VCP} and $UBXL_{OTU1}$ (hereafter referred to as VCP·OTU1) was compared with those of N_{VCP} and UBX_{FAF1} (Ref. 35; Protein Data Bank code 3QQ8; VCP·FAF1) and N_{VCP} and UBD_{NPL4} (Ref. 34; Protein Data Bank code 2PJH; VCP·NPL4). The change in accessible surface area (ΔASA) upon complex formation is 590 $Å^2$ for VCP·OTU1; this is much smaller than the corresponding values for VCP·FAF1 and VCP·NPL4, namely 810 and 1,050 $Å^2$, respectively. The residues involved in the interaction with N_{VCP} are positioned in three regions, namely β1-β2, β3-β4, and β5, as indicated in Fig. 2*C*. The three complex structures are superposed using only the structures of N_{VCP}. Surprisingly, the three VCP-binding partners are at significantly different positions with respect to each other; *i.e.* they do not overlap at all (Fig. 3*A*). The most pronounced difference is in the position of the α1 helix. The relative positioning of the α1 helix from VCP-binding partners is somewhat different as mentioned above (Fig. 2*A*) but is significantly different when the complexes are superimposed; *e.g.* in

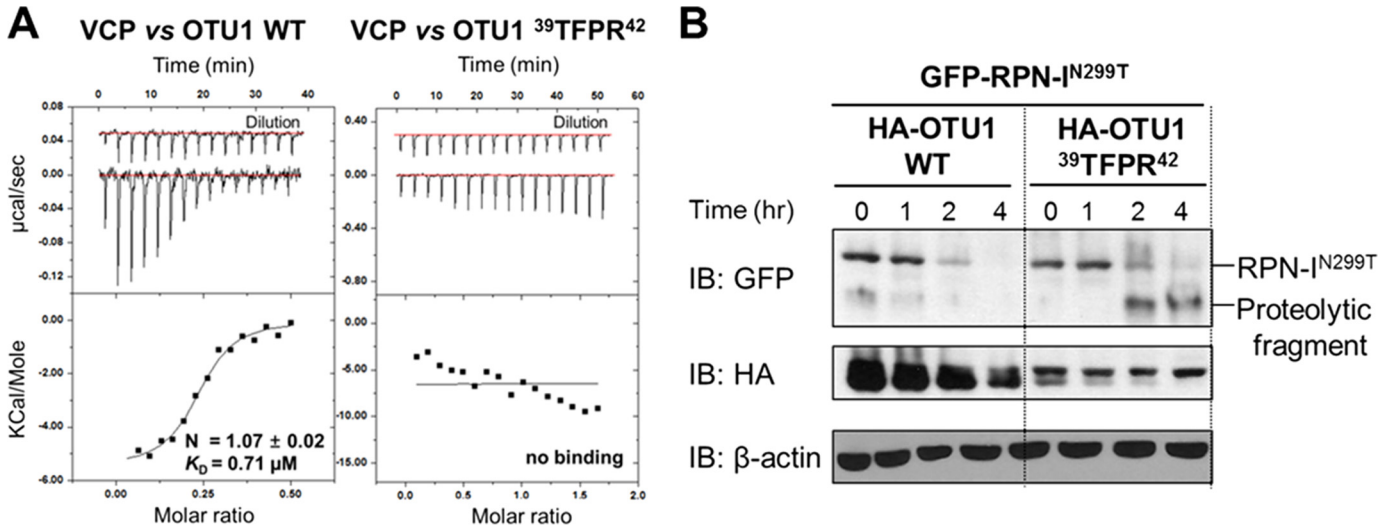

FIGURE 4. **ITC and substrate degradation assay for OTU1 wild type and ^{39}TFPR^{42} mutant.** *A*, ITC raw data and fitted data for the interaction between the full-length VCP and OTU1. The raw data are shown for injection of OTU1 WT (*left*), ^{39}TFPR^{42} (*right*), and a dilution control of OTU1 in buffer (curves on the *top* are offset for clarity). The *lower panels* show the integrated heat data against the molar ratio of VCP to OTU1. The *closed squares* were fitted to a one-site model, and the *solid lines* represent the best fit results. No measurable interaction was detected between VCP and OTU1 ^{39}TFPR^{42}. *B*, influences of OTU1 on degradation of RPN-I^{N299T}. *Left*, OTU1 WT; *right*, OTU1 ^{39}TFPR^{42}. Substrate was totally degraded in the case of OTU1 WT, whereas the degradation process was retarded, resulting in proteolytic fragments, when the S3/S4 loop was mutated. *IB*, immunoblot.

the complex structures, the α1 helix of UBD_{NPL4} is more than 5 Å shifted from that of UBX_{FAF1}, whereas that of $UBXL_{OTU1}$ is somewhat twisted from the other two (Fig. 3*A*).

The molecular surface of N_{VCP} is mapped by interaction of different binding partners (Fig. 3*B*). The binding region common to all three VCP-binding partners is colored in *brown*, the unique surface to $UBXL_{OTU1}$ binding is colored in *blue*, and the region irrelevant to $UBXL_{OTU1}$, *i.e.* relevant to only UBX and UBD, is colored in *green*. As seen in Fig. 3*B*, interaction in the three complexes is in the same general region, but there are clear differences. In particular, Ser^{37} and Arg^{144} of N_{VCP} are only specific to $UBXL_{OTU1}$ binding. They make non-bonded contacts with Tyr^{40} of $UBXL_{OTU1}$, which makes a hydrogen bond to the side chain of Asp^{35} of N_{VCP} (Fig. 3*C*). Interestingly, Tyr^{40} is part of the S3/S4 loop. On the other hand, the *green* region involves residues from the β6-β7 and β11-β12 loops of N_{VCP} that comprise mainly hydrophobic residues. They interact with the residues from the β1-β2 loop of UBX_{FAF1} and UBD_{NPL4}, *i.e.* region 1 (Fig. 2, *A* and *C*). However, the β1-β2 loop of $UBXL_{OTU1}$ clearly adopts a different conformation from the other two (Fig. 2*A*) and does not make any interactions with N_{VCP}, whereas there are numerous interactions involving both hydrophobic and polar residues between N_{VCP} and UBX_{FAF1} (or UBD_{NPL4}) (Fig. 3*B*).

The primary interaction is via the S3/S4 loop of $UBXL_{OTU1}$ as in UBX (Fig. 3*C*). However, binding of $UBXL_{OTU1}$ is somewhat different as the aromatic ring of Tyr^{40} of $UBXL_{OTU1}$ is packed against the following *cis*-Pro^{41} on one side and by the side chains of Val^{38} and Leu^{72} of N_{VCP} on the other side. Also, Tyr^{40} is positioned further between the N1 and N2 domains of N_{VCP}, the hydroxyl oxygen of which makes hydrogen bonds with the carboxyl oxygens of Asp^{35} (2.76 and 3.29 Å) of N_{VCP} (Fig. 3*C*). In addition, arginine in the signature motif of UBX is replaced by threonine in $UBXL_{OTU1}$ and does not seem to be conserved. In the case of VCP·FAF1, the corresponding residue Phe^{619} of UBX_{FAF1} is packed by Val^{38} and Ile^{70} of N_{VCP} on one side, and its carbonyl oxygen makes a hydrogen bond with Arg^{53} of N_{VCP} (3.23 Å). The guanidinium group of Arg^{621} of UBX_{FAF1} makes hydrogen bonds to the carbonyl oxygens of Pro^{137} (3.31 Å) and Leu^{141} (2.52 Å) of N_{VCP}. Alternatively, in UBD_{NPL4}, a 3_{10}-helix is formed instead of the S3/S4 loop found in UBX_{FAF1} and $UBXL_{OTU1}$, and this facilitates N_{VCP} binding (Figs. 2*C* and 3*C*). Another major interaction region involves the C-terminal region of the binding partners (Fig. 2*C*). They interact with Phe^{52}, Arg^{53}, Gly^{54}, and Asp^{55} of N_{VCP}, which is colored in *brown* (Fig. 3*B*). As seen in the figure, this region is equally important. However, the degree of interactions varies per the three complex structures. For example, Arg^{53} of N_{VCP} makes six hydrogen bonds in VCP·OTU1, whereas the same residue of N_{VCP} forms only three and two hydrogen bonds in VCP·FAF1 and VCP·NPL4, respectively. Taken together, our data show that $UBXL_{OTU1}$ binds in a similar position of N_{VCP} as UBX_{FAF1} and UBD_{NPL4}, but the interaction mode is specific unlike the others. This implies that OTU1 is a particular binding partner of VCP.

The S3/S4 Loop of OTU1 Critical for VCP Binding and the ERAD Pathway—To confirm the importance of the S3/S4 loop of OTU1 in VCP binding based on the complex structure, the mutant was made by using the full-length OTU1. The S3/S4 loop of OTU1 was replaced with that of FAF1, which showed the closest resemblance as shown above; *i.e.* the mutant (OTU1 ^{39}TFPR^{42}) has the S3/S4 loop sequence corresponding to Thr^{618}-Phe-Pro-Arg^{621} of FAF1. The interactions between the full-length VCP and OTU1 were measured using ITC, and the results are shown in Fig. 4*A*. The binding affinity (K_D) between VCP and OTU1 WT is 0.71 μM, whereas the corresponding value for OTU1 ^{39}TFPR^{42} could not be measured possibly due to weak binding. This could be understood based on the modeling study, which showed physical clashes with N_{VCP} when the Gly-Tyr-Pro-Pro loop of OTU1 was replaced by Thr-Phe-Pro-

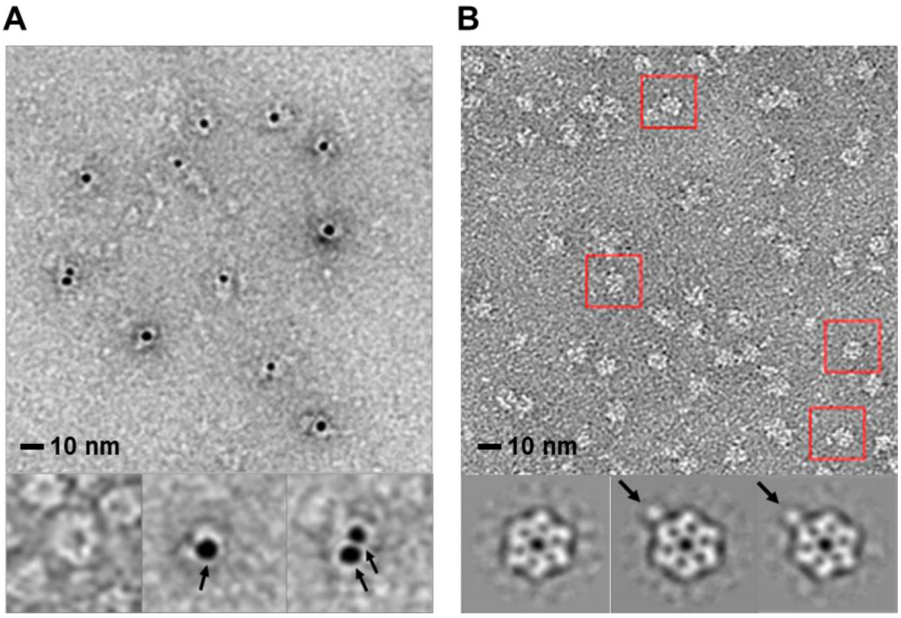

FIGURE 5. **EM analysis on single particle of the VCP and OTU1 complex.** *A*, raw images of VCP complexed with gold-labeled OTU1. *Bottom panels* show VCP with no label as a control (*left*) and particles with one (*middle*) and two (*right*) gold particles with *black arrows* indicating the gold particle. *B*, electron micrograph of the VCP and OTU1 complex. The *bottom panel* shows the representative two-dimensional class average for VCP alone (*left*) and VCP/OTU1 complex (*middle* and *right*). VCP/OTU1 complex is marked by a *red box*. The *arrow* indicates the OTU1 molecule.

Arg (data not shown). In addition, the two prolines in the S3/S4 loop of OTU1 may impose rigidity in the backbone conformation and prevent conformational changes from propagating to the rest of the protein. The substitution of proline with other residues such as glycine or arginine relieves the rigidity of the backbone and increases the flexibility of the loop. Therefore, forming a negative loop of $UBXL_{OTU1}$ leads to low binding affinity between VCP and OTU1.

A substrate degradation assay was carried out to check whether the inability of OTU1 binding to VCP has any influence on the ERAD pathway using ribophorin I (RPN-I^{N299T}) as an ERAD substrate. Degradation of the substrate was monitored in the presence of cycloheximide (37). OTU1 ^{39}TFPR^{42} showed relatively reduced degradation and accumulation of RPN-I^{N299T} in comparison with OTU1 WT (Fig. 4*B*). This result shows that disruption of the association between VCP and OTU1 leads to the negative regulation of the ERAD pathway; thus, the S3/S4 loop of OTU1 is highly specific and is involved in a unique association with VCP.

It has been reported previously that abrogation of the deubiquitinating activity of OTU1 resulted in impairment of the degradation of misfolded RI332 as an ERAD substrate, suggesting that OTU1 positively regulates the ERAD pathway (13). Here, although $UBXL_{OTU1}$ has no relation to the enzymatic activity of OTU1, disruption of the interaction between VCP and OTU1 led to defects in the degradation of ERAD substrates. Therefore, it seems that $UBXL_{OTU1}$ is required for the ERAD pathway. Likewise, recent reports have suggested the importance of the association of VCP and UBX-containing proteins. For instance, the S3/S4 loop mutant of UBX_{FAF1} lost the ability to interact with VCP as well as with ubiquitinated substrate via its ubiquitin-associated domain, resulting in the accumulation of substrate (38). Another example is UBXD7, which separately binds both VCP and substrate HIF1α and recruits the substrate to VCP for degradation. However, its UBX-lacking mutant could not interact with both VCP and substrate, thus leading to a defect in the degradation of HIF1α (39). Therefore, the association of UBX-containing proteins with VCP is involved in their function; *i.e.* binding of OTU1 to VCP is needed to activate OTU1 in the ERAD pathway, demonstrating the importance of $UBXL_{OTU1}$. Furthermore, the S3/S4 loop of OTU1 is conserved as residues Gly-Tyr/Phe-Pro-Pro are found in other OTU1 homologs and VCP complex-interacting protein of 135 kDa (VCIP135) which is another known UBXL-containing protein (Refs. 40 and 41 and data not shown). Therefore, not only VCIP135 but also OTU1 homologs are expected to bind VCP in the same manner shown in this study.

Interaction between the Full-length Proteins—Because VCP exists as a homohexamer, it can possibly bind six different binding partners. Therefore, it is important to characterize the stoichiometry and interaction between the full-length VCP and its binding partners. To determine the stoichiometry of VCP and OTU1, an EM study was carried out. First, gold labeling was carried out using a hexahistidine tag. The tag was added to the C terminus of OTU1 because its N-terminal domain binds to VCP. Negative staining EM images of VCP alone and in complex with the gold-labeled OTU1 were taken. About 5,800 single particles were selected from individual micrographs, and the stoichiometry between VCP and OTU1 was analyzed statistically by counting the number of gold particles. Approximately 80% of the selected particles had one gold particle, and about 15% had two (Fig. 5*A*). The remaining 5% were particles with more than three gold particles (data not shown). We then took images of the complex of the full-length proteins (VCP/OTU1 complex) without gold labeling to avoid the restrictive space constraints due to the gold particle, which has a diameter of 5 nm. Three types of negative staining solutions were tried, but methylamine vanadate, pH 8.0 gave the best result as shown

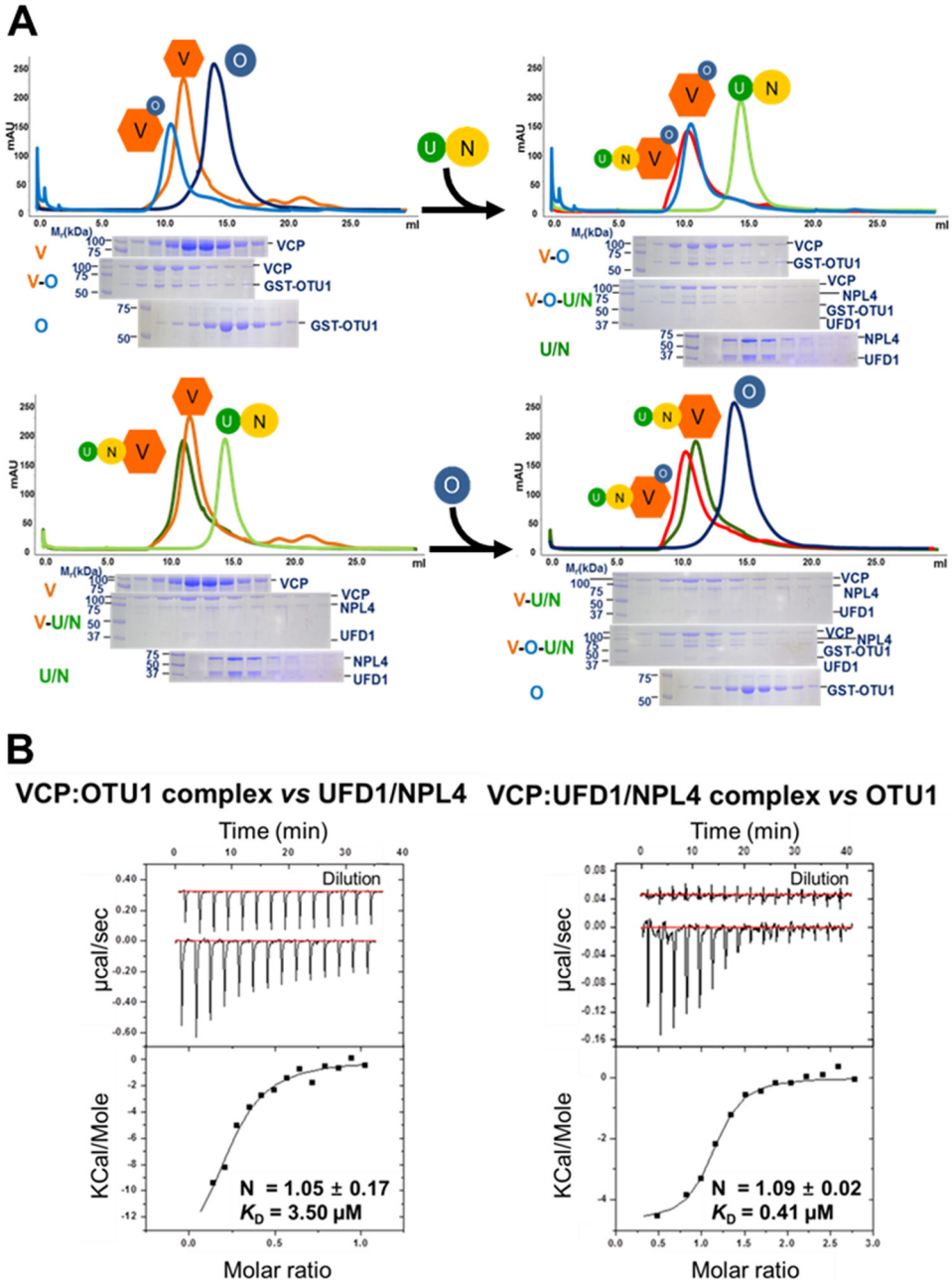

FIGURE 6. **Dependence test of OTU1 binding to VCP on UFD1/NPL4.** *A*, size exclusion chromatography profile and Coomassie-stained SDS-PAGE of fractions of VCP, GST-OTU1, and UFD1/NPL4. To hexameric VCP, GST-OTU1 and UFD1/NPL4 (*top*) and UFD1/NPL4 and GST-OTU1 (*bottom*) were added. SDS-PAGE fractions are shown below the chromatograms. *V*, *O*, *U*, and *N* stand for VCP, OTU1, UFD1, and NPL4. *B*, ITC binding data for UFD1/NPL4 binding to VCP/OTU1 complex (*left*) and for OTU1 binding to VCP·UFD1/NPL4 complex (*right*). *mAU*, milli-absorbance units.

in Fig. 5*B*. A total of 2,452 particles of VCP/OTU1 complex were separated successfully from 2,839 particles of a mixture containing VCP alone and VCP/OTU1 complex with the class average. When uranyl formate was used, the ratio between the complex and VCP alone was almost 1,134 to 4,231 possibly due to the acidic nature of the solution, namely pH 5.5 (data not shown). Representative two-dimensional class averages for VCP alone and VCP/OTU1 complex are shown in Fig. 5*B*, which clearly shows that one OTU1 molecule binds to one vertex of homohexameric VCP. ITC measurement using the full-length VCP and OTU1 showed a binding stoichiometry of $n = 1.07 \pm 0.02$ and a K_D of 0.71 μM, suggesting that the stoichiometry of OTU1 to VCP is near 1:6. This is in good agreement with the EM data above. In addition, when $UBXL_{OTU1}$ was removed (data not shown) or mutated (Fig. 4*A*), it did not show measurable binding to VCP. This confirmed again that $UBXL_{OTU1}$ is necessary for binding to VCP.

The stoichiometries between VCP and various binding partners have been reported. In the case of UFD1/NPL4, EM studies clearly show that one UFD1/NPL4 binds one VCP hexamer (5, 42). On the contrary, for both p47 and UBXD1, three molecules of each bind to one VCP hexamer (43, 44). Interestingly, in the case of both FAF1 and UBXD7, one molecule binds one VCP hexamer only when UFD1/NPL4 is prebound to VCP (35, 38).

The K_D values of VCP and its binding partners are 1.7 μM for UFD1/NPL4 (35), 2.3 μM for FAF1 (35), 3.1 μM for UBXD7 (35), and 0.5 μM for p47 (43). These values are comparable with what we have seen with OTU1. It is worthwhile mentioning that in some cases bipartite binding has been reported. For example, VCP binding of UFD1/NPL4 utilizes the BS1 segment, which is a short hydrophobic stretch in the C-terminal domain of UFD1, in addition to the UBD of NPL4 as described above (45). Also, p47 uses a shp1-eyc-p47 domain, which is in the middle of p47, in addition to the C-terminal UBX domain. The shp1-eyc-p47 domain is reported to form a trimer and binds at the interface between the N and D1 domains of VCP. Besides the hierarchical binding of VCP-binding partners, some binding partners such as UFD1/NPL4, p47, and UBXD1 are reported to show mutually exclusive binding (46, 47), whereas others such as UFD1/NPL4 and UBX4 show simultaneous binding (48). This is understandable considering the existence of numerous binding partners and the diverse functions of VCP. Although the crystal structure of truncated proteins showed 1:1 binding between $UBXL_{OTU1}$ and N_{VCP}, the EM study using the full-length proteins clearly showed that one OTU1 binds to the hexameric VCP, suggesting only one OTU1 molecule is sufficient to perform its function; furthermore, it may function with other binding partners.

Dependence of OTU1 Binding to VCP on VCP Adaptor Proteins UFD1/NPL4—UFD1/NPL4 plays a crucial role in the ERAD pathway together with VCP, and some VCP-binding partners show hierarchical binding as well as mutually exclusive binding to VCP. We tested the binding pattern for VCP between OTU1 and UFD1/NPL4 using size exclusion chromatography and ITC, and the results are shown in Fig. 6. A GST-tagged OTU1 (GST-OTU1) was used to avoid possible confusion caused by molecular weights on size exclusion chromatography and SDS-PAGE. Two sets of experiments were carried out. First, GST-OTU1 was added to VCP alone, and then UFD1/NPL4 was added. Second, UFD1/NPL4 was added to VCP alone, and then OTU1 was added. As expected, both OTU1 and UFD1/NPL4 form a complex with VCP alone, but in addition, both form a quaternary complex, *i.e.* VCP·GST-OTU1·UFD1/NPL4 (Fig. 6*A*). We further determined the binding affinities and the stoichiometries between these using ITC, and the results are shown in Fig. 6*B*. First, UFD1/NPL4 and premade VCP/OTU1 binary complex showed an apparent K_D of 3.50 μM and $n = 1.05 \pm 0.17$, whereas OTU1 and premade VCP·UFD1/NPL4 ternary complex gave a K_D of 0.41 μM and $n = 1.09 \pm 0.02$. Both suggest that there is 1:1 binding. Interestingly, the K_D values are similar to those obtained for VCP alone; *e.g.* the K_D for UFD1/NPL4 binding to VCP was reported as 1.7 μM (35), and the K_D for OTU1 binding to VCP was 0.71 μM (see Fig. 4*A*). This clearly shows that VCP can bind OTU1 in both the presence and absence of UFD1/NPL4 and vice versa.

In summary, we have dissected the interaction between VCP and OTU1. One OTU1 molecule binds to one VCP hexamer with similar binding affinity both in the presence and absence of UFD1/NPL4. The $UBXL_{OTU1}$ binds at the interface between the two subdomains (N1 and N2) of VCP. In particular, the conformation of the Gly^{39}-Tyr^{40}-*cis*-Pro^{41}-Pro^{42} loop of $UBXL_{OTU1}$ is critical for N_{VCP} binding. Although some of these properties of UBXL mimic UBX, the interaction is quite specific and has direct bearing on the proteasomal degradation of ERAD substrates. Based on these results, it is plausible that OTU1 can participate in the regulation of ubiquitinated substrates in both UFD1/NPL4-dependent and -independent manners. Our data provide insights into the interaction between the full-length VCP and OTU1 as well as the interaction between N_{VCP} and $UBXL_{OTU1}$ that could be applicable to other UBXL-containing proteins.

Acknowledgments—We thank the staff at 5C beamline, Pohang Accelerator Laboratory, Republic of Korea; Professor Y. K. Kang for interpreting the conformation of the loop; Dr. J. K. Park for VCP, UFD1, and NPL4 constructs; and S.-G. Lee for help with the EM study.

REFERENCES

1. Ciechanover, A. (2005) Proteolysis: from the lysosome to ubiquitin and the proteasome. *Nat. Rev. Mol. Cell Biol.* **6,** 79–87
2. de Vrij, F. M., Fischer, D. F., van Leeuwen, F. W., and Hol, E. M. (2004) Protein quality control in Alzheimer's disease by the ubiquitin proteasome system. *Prog. Neurobiol.* **74,** 249–270
3. Bagola, K., Mehnert, M., Jarosch, E., and Sommer, T. (2011) Protein dislocation from the ER. *Biochim. Biophys. Acta* **1808,** 925–936
4. Wolf, D. H., and Stolz, A. (2012) The Cdc48 machine in endoplasmic reticulum associated protein degradation. *Biochim. Biophys. Acta* **1823,** 117–124
5. Bebeacua, C., Förster, A., McKeown, C., Meyer, H. H., Zhang, X., and Freemont, P. S. (2012) Distinct conformations of the protein complex p97-Ufd1-Npl4 revealed by electron cryomicroscopy. *Proc. Natl. Acad. Sci. U.S.A.* **109,** 1098–1103
6. Gille, C., Lorenzen, S., Michalsky, E., and Frömmel, C. (2003) KISS for STRAP: user extensions for a protein alignment editor. *Bioinformatics* **19,** 2489–2491
7. DeLaBarre, B., and Brunger, A. T. (2003) Complete structure of p97/valosin-containing protein reveals communication between nucleotide domains. *Nat. Struct. Biol.* **10,** 856–863
8. Yamanaka, K., Sasagawa, Y., and Ogura, T. (2012) Recent advances in p97/VCP/Cdc48 cellular functions. *Biochim. Biophys. Acta* **1823,** 130–137
9. Meyer, H., Bug, M., and Bremer, S. (2012) Emerging functions of the VCP/p97 AAA-ATPase in the ubiquitin system. *Nat. Cell Biol.* **14,** 117–123
10. Jentsch, S., and Rumpf, S. (2007) Cdc48 (p97): a "molecular gearbox" in the ubiquitin pathway? *Trends Biochem. Sci.* **32,** 6–11
11. Goder, V. (2012) Roles of ubiquitin in endoplasmic reticulum-associated protein degradation (ERAD). *Curr. Protein Pept. Sci.* **13,** 425–435
12. Liu, Y., and Ye, Y. (2012) Roles of p97-associated deubiquitinases in protein quality control at the endoplasmic reticulum. *Curr. Protein Pept. Sci.* **13,** 436–446
13. Ernst, R., Mueller, B., Ploegh, H. L., and Schlieker, C. (2009) The otubain YOD1 is a deubiquitinating enzyme that associates with p97 to facilitate protein dislocation from the ER. *Mol. Cell* **36,** 28–38
14. Bernardi, K. M., Williams, J. M., Inoue, T., Schultz, A., and Tsai, B. (2013) A deubiquitinase negatively regulates retro-translocation of non-ubiquitinated substrates. *Mol. Biol. Cell* **24,** 3545–3556
15. Rumpf, S., and Jentsch, S. (2006) Functional division of substrate processing cofactors of the ubiquitin-selective Cdc48 chaperone. *Mol. Cell* **21,** 261–269
16. Schuberth, C., and Buchberger, A. (2008) UBX domain proteins: major regulators of the AAA ATPase Cdc48/p97. *Cell. Mol. Life Sci.* **65,** 2360–2371
17. Kloppsteck, P., Ewens, C. A., Förster, A., Zhang, X., and Freemont, P. S. (2012) Regulation of p97 in the ubiquitin-proteasome system by the UBX protein-family. *Biochim. Biophys. Acta* **1823,** 125–129

18. Messick, T. E., Russell, N. S., Iwata, A. J., Sarachan, K. L., Shiekhattar, R., Shanks, J. R., Reyes-Turcu, F. E., Wilkinson, K. D., and Marmorstein, R. (2008) Structural basis for ubiquitin recognition by the Otu1 ovarian tumor domain protein. *J. Biol. Chem.* **283,** 11038–11049
19. Mevissen, T. E., Hospenthal, M. K., Geurink, P. P., Elliott, P. R., Akutsu, M., Arnaudo, N., Ekkebus, R., Kulathu, Y., Wauer, T., El Oualid, F., Freund, S. M., Ovaa, H., and Komander, D. (2013) OTU deubiquitinases reveal mechanisms of linkage specificity and enable ubiquitin chain restriction analysis. *Cell* **154,** 169–184
20. Otwinowski, Z., and Minor, W. (1997) Processing of x-ray diffraction data collected in oscillation mode. *Methods Enzymol.* **276**, 307–326
21. McCoy, A. J., Grosse-Kunstleve, R. W., Adams, P. D., Winn, M. D., Storoni, L. C., and Read, R. J. (2007) Phaser crystallographic software. *J. Appl. Crystallogr.* **40,** 658–674
22. Zhang, X., Shaw, A., Bates, P. A., Newman, R. H., Gowen, B., Orlova, E., Gorman, M. A., Kondo, H., Dokurno, P., Lally, J., Leonard, G., Meyer, H., van Heel, M., and Freemont, P. S. (2000) Structure of the AAA ATPase p97. *Mol. Cell* **6,** 1473–1484
23. Emsley, P., and Cowtan, K. (2004) Coot: model-building tools for molecular graphics. *Acta Crystallogr. D Biol. Crystallogr.* **60,** 2126–2132
24. Brünger, A. T., Adams, P. D., Clore, G. M., DeLano, W. L., Gros, P., Grosse-Kunstleve, R. W., Jiang, J. S., Kuszewski, J., Nilges, M., Pannu, N. S., Read, R. J., Rice, L. M., Simonson, T., and Warren, G. L. (1998) Crystallography & NMR system: a new software suite for macromolecular structure determination. *Acta Crystallogr. D Biol. Crystallogr.* **54,** 905–921
25. Zwart, P. H., Afonine, P. V., Grosse-Kunstleve, R. W., Hung, L. W., Ioerger, T. R., McCoy, A. J., McKee, E., Moriarty, N. W., Read, R. J., Sacchettini, J. C., Sauter, N. K., Storoni, L. C., Terwilliger, T. C., and Adams, P. D. (2008) Automated structure solution with the PHENIX suite. *Methods Mol. Biol.* **426,** 419–435
26. Murshudov, G. N., Vagin, A. A., and Dodson, E. J. (1997) Refinement of macromolecular structure by the maximum-likelihood method. *Acta Crystallogr. D Biol. Crystallogr.* **53,** 240–255
27. Laskowski, R. A., MacArthur, M. W., Moss, D. S., and Thornton, J. M. (1993) PROCHECK: a program to check the stereochemical quality of protein structures. *J. Appl. Crystallogr.* **26,** 283–291
28. DeLano, W. L. (2010) *The PyMOL Molecular Graphics System*, version 1.3r1, Schrödinger, LLC, New York
29. Tang, G., Peng, L., Baldwin, P. R., Mann, D. S., Jiang, W., Rees, I., and Ludtke, S. J. (2007) EMAN2: an extensible image processing suite for electron microscopy. *J. Struct. Biol.* **157,** 38–46
30. van Heel, M., Harauz, G., Orlova, E. V., Schmidt, R., and Schatz, M. (1996) A new generation of the IMAGIC image processing system. *J. Struct. Biol.* **116,** 17–24
31. Huyton, T., Pye, V. E., Briggs, L. C., Flynn, T. C., Beuron, F., Kondo, H., Ma, J., Zhang, X., and Freemont, P. S. (2003) The crystal structure of murine p97/VCP at 3.6 Å. *J. Struct. Biol.* **144,** 337–348
32. van der Veen, A. G., and Ploegh, H. L. (2012) Ubiquitin-like proteins. *Annu. Rev. Biochem.* **81,** 323–357
33. Bang, D., Makhatadze, G. I., Tereshko, V., Kossiakoff, A. A., and Kent, S. B. (2005) Total chemical synthesis and x-ray crystal structure of a protein diastereomer: [D-Gln35] ubiquitin. *Angew. Chem. Int. Ed. Engl.* **44,** 3852–3856
34. Isaacson, R. L., Pye, V. E., Simpson, P., Meyer, H. H., Zhang, X., Freemont, P. S., and Matthews, S. (2007) Detailed structural insights into the p97-Npl4-Ufd1 interface. *J. Biol. Chem.* **282,** 21361–21369
35. Hänzelmann, P., Buchberger, A., and Schindelin, H. (2011) Hierarchical binding of cofactors to the AAA ATPase p97. *Structure* **19,** 833–843
36. Dreveny, I., Kondo, H., Uchiyama, K., Shaw, A., Zhang, X., and Freemont, P. S. (2004) Structural basis of the interaction between the AAA ATPase p97/VCP and its adaptor protein p47. *EMBO J.* **23,** 1030–1039
37. de Virgilio, M., Kitzmüller, C., Schwaiger, E., Klein, M., Kreibich, G., and Ivessa, N. E. (1999) Degradation of a short-lived glycoprotein from the lumen of the endoplasmic reticulum: the role of N-linked glycans and the unfolded protein response. *Mol. Biol. Cell* **10,** 4059–4073
38. Lee, J. J., Park, J. K., Jeong, J., Jeon, H., Yoon, J. B., Kim, E. E., and Lee, K. J. (2013) Complex of Fas-associated factor 1 (FAF1) with valosin-containing protein (VCP)-Npl4-Ufd1 and polyubiquitinated proteins promotes endoplasmic reticulum-associated degradation (ERAD). *J. Biol. Chem.* **288,** 6998–7011
39. Alexandru, G., Graumann, J., Smith, G. T., Kolawa, N. J., Fang, R., and Deshaies, R. J. (2008) UBXD7 binds multiple ubiquitin ligases and implicates p97 in HIF1α turnover. *Cell* **134,** 804–816
40. Uchiyama, K., Jokitalo, E., Kano, F., Murata, M., Zhang, X., Canas, B., Newman, R., Rabouille, C., Pappin, D., Freemont, P., and Kondo, H. (2002) VCIP135, a novel essential factor for p97/p47-mediated membrane fusion, is required for Golgi and ER assembly *in vivo*. *J. Cell Biol.* **159,** 855–866
41. Uchiyama, K., Totsukawa, G., Puhka, M., Kaneko, Y., Jokitalo, E., Dreveny, I., Beuron, F., Zhang, X., Freemont, P., and Kondo, H. (2006) p37 is a p97 adaptor required for Golgi and ER biogenesis in interphase and at the end of mitosis. *Dev. Cell* **11,** 803–816
42. Pye, V. E., Beuron, F., Keetch, C. A., McKeown, C., Robinson, C. V., Meyer, H. H., Zhang, X., and Freemont, P. S. (2007) Structural insights into the p97-Ufd1-Npl4 complex. *Proc. Natl. Acad. Sci. U.S.A.* **104,** 467–472
43. Beuron, F., Dreveny, I., Yuan, X., Pye, V. E., McKeown, C., Briggs, L. C., Cliff, M. J., Kaneko, Y., Wallis, R., Isaacson, R. L., Ladbury, J. E., Matthews, S. J., Kondo, H., Zhang, X., and Freemont, P. S. (2006) Conformational changes in the AAA ATPase p97-p47 adaptor complex. *EMBO J.* **25,** 1967–1976
44. Hänzelmann, P., and Schindelin, H. (2011) The structural and functional basis of the p97/valosin-containing protein (VCP)-interacting motif (VIM): mutually exclusive binding of cofactors to the N-terminal domain of p97. *J. Biol. Chem.* **286,** 38679–38690
45. Bruderer, R. M., Brasseur, C., and Meyer, H. H. (2004) The AAA ATPase p97/VCP interacts with its alternative co-factors, Ufd1-Npl4 and p47, through a common bipartite binding mechanism. *J. Biol. Chem.* **279,** 49609–49616
46. Chia, W. S., Chia, D. X., Rao, F., Bar Nun, S., and Geifman Shochat, S. (2012) ATP binding to p97/VCP D1 domain regulates selective recruitment of adaptors to its proximal N-domain. *PLoS One* **7,** e50490
47. Kern, M., Fernandez-Sáiz, V., Schäfer, Z., and Buchberger, A. (2009) UBXD1 binds p97 through two independent binding sites. *Biochem. Biophys. Res. Commun.* **380,** 303–307
48. Alberts, S. M., Sonntag, C., Schäfer, A., and Wolf, D. H. (2009) Ubx4 modulates cdc48 activity and influences degradation of misfolded proteins of the endoplasmic reticulum. *J. Biol. Chem.* **284,** 16082–16089
49. Gouet, P., Courcelle, E., Stuart, D.I., and Métoz, F. (1999) ESPript: analysis of multiple sequence alignments in PostScript. *Bioinformatics* **15,** 305–308